Novel Ternary Metals-based Telluride Electrocatalyst with Synergistic Effects of High Valence Non-3d Metal and Oxophilic Te for pH-Universal Hydrogen Evolution Reaction

Seunghwan Jo[a], Wenxiang Liu[b], Yanan Yue[b], Ki Hoon Shin[a], Keon Beom Lee[a], Hyeonggeun Choi[a], Bo Hou[c,], and Jung Inn Sohn[a,*]*

[a] Division of Physics and Semiconductor Science, Dongguk University, Seoul 04620, Republic of Korea

[b] School of Power and Mechanical Engineering, Wuhan University, Wuhan, Hubei 430072, China

[c] School of Physics and Astronomy, Cardiff University, Cardiff, CF24 3AA, Wales, UK

* Corresponding authors (Prof. Bo Hou and Prof. Jung Inn Sohn)

E-mail: Houb6@cardiff.ac.uk and junginn.sohn@dongguk.edu

Keywords: telluride catalyst, oxophilic effect, high valence non-3d metal, bifunctional mechanism, pH-universal hydrogen evolution reaction

ABSTRACT

Electrocatalyst designs based on oxophilic foreign atoms are considered a promising approach for developing efficient pH-universal hydrogen evolution reaction (HER) electrocatalysts by overcoming the sluggish alkaline HER kinetics. Here, we design ternary transition metals-based nickel telluride (MoWNiTe) catalysts consisting of high valence non-3d Mo and W metals and oxophilic Te as a first demonstration of non-precious heterogeneous electrocatalysts following the bifunctional mechanism. The MoWNiTe showed excellent HER catalytic performance with overpotentials of 72, 125, and 182 mV to reach the current densities of 10, 100, and 1000 mA cm^{-2}, respectively, and the corresponding Tafel slope of 47, 52, and 58 mV dec^{-1} in alkaline media, which is much superior to commercial Pt/C. Additionally, the HER performance of MoWNiTe is well maintained up to 3000 hours at the current density of 100 mA cm^{-2}. It is further demonstrated that the MoWNiTe exhibits remarkable HER activities with an overpotential of 45 mV (31 mV) and Tafel slope of 60 mV dec^{-1} (34 mV dec^{-1}) at 10 mA cm^{-2} in neutral (acid) media. The superior HER performance of MoWNiTe is attributed to the electronic structure modulation, inducing highly active low valence states by the incorporation of high valence non-3d transition metals. It is also attributed to the oxophilic effect of Te, accelerating water dissociation kinetics through a bifunctional catalytic mechanism in alkaline media. Density functional theory calculations further reveal that such synergistic effects lead to reduced free energy for an efficient water dissociation process, resulting in remarkable HER catalytic performances within universal pH environments.

1. Introduction

Hydrogen fuel (H_2) generated by electrochemical water splitting has been considered a potential alternative to traditional fossil fuels, to address the energy crisis and global warming, due to its outstanding energy density and eco-friendly manufacturability [1-3]. Considerable effort has been focused on designing and realizing high-efficiency and enduring electrocatalysts for efficient renewable energy conversion. However, for genuine practical applications, overcoming the energy barrier associated with sluggish reaction kinetics for water dissociation remains challenging, which requires a higher potential than the theoretical value [4-7]. In particular, the hydrogen evolution reaction (HER) kinetics in alkaline media is much slower than that in its acidic counterpart. This is attributed to its multi-step reaction pathway based on a combination of the Volmer and Heyrovsky steps or the Volmer and Tafel steps where the overall kinetics is limited by the sluggish Volmer step ($H_2O + e^- \rightarrow H_{ad} + OH^-$).

Recent studies have demonstrated that the incorporation of oxophilic metals into the catalyst composition is crucial to enhancing the alkaline HER activity, leading to the contribution of faster kinetics in the rate-determining Volmer step. Accordingly, modifying the catalytic surface with foreign metals that have a higher oxophilicity is the most preferred approach to providing bifunctional catalytic sites for efficient HER in non-acidic media, eventually for pH-universal HER [8-14]. However, most of the studies that carried out the bifunctional theory based on the oxophilic effect were limited to the high cost and reserve scarcity of noble Pt-based electrocatalysts [15,16]. Thus, it is highly desirable to consider the extension of the bifunctional effect to more economic non-precious catalysts. In principle, from a viewpoint of surface modification of catalysts design, the combination of earth-abundant active transition metals and foreign elements with low effective nuclear charges and electronegativities can synergistically accelerate the alkaline HER kinetics due to the introduction of oxophilicity. In this regard, earth-abundant transition metal chalcogenides (TMCs) are one of the materials that can be used to enhance alkaline HER activity through the modification of catalytic surface and the chemical environment through broad-range phases with tunable composition [17-20]. Among the chalcogens, similar to metal cations with oxophilic properties, tellurium (Te) would be a viable option for exploiting new TMCs materials following the bifunctional theory. This is because Te is semi-metallic and possesses low electronegativity and high electrical conductivity but has received little interest in the field of oxophilic catalyst systems to date [21-24].

In this study, we designed and synthesized a ternary transition metals-based telluride system (MoWNiTe) as a new class of electrocatalysts in which oxophilic Te acts as a bifunctional catalytic site. We found that the combined incorporation of high valence non-3d two Mo and W metals into heterogeneous catalyst systems enables an effective modulation of the electronic structure, leading to electron-rich low valence states, and the synthesis of relatively small particles with large catalytic surface area by reducing the overgrowth through sluggish atomic diffusion. Moreover, it is found that Te also provides oxophilic properties, which can significantly improve catalytic performance based on the bifunctional catalytic mechanism associated with the accumulation ability of reactive OH* species on the catalytic surface in alkaline media. These experimental results were further confirmed by density functional theory calculations showing that the free energy associated with water dissociation can be decreased through a combination of high valence non-3d metals and oxophilic Te.

2. Experimental

2.1 Solution preparation

Nickel nitrate hexahydrate ($Ni(NO_3)_2 \cdot 6H_2O$), tellurium dioxide (TeO_2), sodium molybdate dihydrate ($Na_2MoO_4 \cdot 2H_2O$), sodium tungstate dihydrate ($Na_2WO_4 \cdot 2H_2O$), and ethanolamine (C_2H_7NO) were purchased from Sigma Aldrich and were used without further purification. Four different solutions were prepared for the electrochemical deposition process. 1 mM of $Ni(NO_3)_2 \cdot 6H_2O$ and TeO_2 were dissolved in 28 mL of DI water, and then 2 mL of C_2H_7NO was added (denoted as a NiTe solution). 1 mM of $Ni(NO_3)_2 \cdot 6H_2O$, and $Na_2MoO_4 \cdot 2H_2O$ (or $Na_2WO_4 \cdot 2H_2O$) were dissolved in 28 mL of DI water, and then 2 mL of C_2H_7NO was added (denoted as MoNi, and WNi solutions). 1 mM of $Ni(NO_3)_2 \cdot 6H_2O$, $Na_2MoO_4 \cdot 2H_2O$, and $Na_2WO_4 \cdot 2H_2O$ were dissolved in 28 mL of DI water, and then 2 mL of C_2H_7NO was added (denoted as a MoWNi solution).

2.2 Electrochemical deposition

The electrochemical deposition was conducted at 40 °C using Autolab potentiostat PGSTAT302N. A pair of nickel foams were used as the cathode and anode in a two-electrode system, and the solutions were used as electrolytes [25]. The working electrode was subjected to current densities of + 30 mA cm^{-2} and – 30 mA cm^{-2} for 5 minutes in turns using the NiTe solution as an electrolyte.

The resulting NiTe electrode was washed with DI water and directly used for secondary deposition. To obtain MoWNiTe, a current density of - 30 mA cm^{-2} was applied to the NiTe electrode for 10 minutes using the MoWNi solution as the electrolyte. Similarly, to obtain MoNiTe, and WNiTe, a current density of - 30 mA cm^{-2} was applied to the NiTe electrode for 10 minutes but using the MoNi and WNi solution as electrolytes, respectively. Overgrown NiTe was prepared under the same synthetic condition without solution change. All the electrodes were washed with DI water after the electrochemical deposition process and dried at 60 ℃ overnight. To demonstrate the catalytic role of Te in MoWNiTe, the dissolved amount of Te precursors in electrolyte solutions for electrochemical deposition was controlled by varying molar concentrations of Te precursors from 1, 0.75, 0.5, 0.25, and 0 mM, denoted as 100 % (MoWNiTe), 75 % ($MoWNiTe_{0.75}$), 50 % ($MoWNiTe_{0.50}$), 25 % ($MoWNiTe_{0.25}$), and 0 % (MoWNi), respectively.

2.3 Material Characterization

Field emission scanning electron microscope (JSM-7800F Prime, JEOL Ltd, Japan), and spherical aberration-corrected transmission electron microscope (JEM-ARM200F, JEOL Ltd, Japan) were used to investigate morphologies and atomic arrangements of the samples. Energy-dispersive X-ray spectroscope (EDS) and Cs-TEM measurements were performed to identify the elemental distribution of electrodeposited catalysts. The chemical structural properties of catalyst samples were investigated by using X-ray photoelectron spectroscope (ULVAC PHI 5000 VersaProbe II, ThermoFisher Scientific, UK). All the binding energies were calibrated to C 1s (284.8 eV) to avoid any misunderstanding originating from an instrumental error. The crystal structure of the samples was examined by X-ray diffraction (Ultima IV, Rigaku, Japan) analysis. Zeta potentials were measured using a zeta potential analyzer (ELSZ2000, OTSUKA, Japan). Inductively coupled plasma atomic emission spectrometer (ICP-AES, OPTIMA 8300, Perkin-Elmer, USA) was used to estimate the elemental composition of electrodeposited catalysts.

2.4 Electrochemical measurements

Before electrochemical measurements, all the samples were chemically activated by immersing in a 6 M KOH solution purged with Ar gas at room temperature for 5 minutes. The activated samples were washed with DI water and directly used as a working electrode. Electrochemical measurements were performed in a three-electrode system composed of the working electrode, Pt counter electrode, and reference electrode. Hg/HgO (20 % KOH, 0.098 V) was used as the

reference electrode in alkaline media, and Ag/AgCl (Saturated KCl, 0.197 V) as the reference electrode in neutral and acidic media. Commercial Pt/C was prepared as a comparison for HER applications. 10 mg of commercial Pt/C (Sigma Aldrich) was immersed in 950 µL of isopropanol alcohol and then 50 µL of 5 wt% of nafion solution was added. 200 µL of the homogeneously mixed solution was dropped poured on the nickel foam surface and dried at 60 ℃ overnight.

The reversible hydrogen electrode (RHE) was calculated using Equation 1.

$$E_{RHE} = E_{ref} + 0.059 * pH + E°_{ref} \quad (1)$$

All potential values were iR-corrected using solution resistance (R_s) values measured by electrochemical impedance spectroscopy (EIS). The EIS was conducted at – 0.1 V versus RHE with a frequency range from 10 kHz to 10 mHz. Electrochemical active surface areas (ECSAs) were calculated using Equation 2.

$$ECSAs = C_{dl} / C_s \quad (2)$$

C_{dl} represents double-layer capacitance, and C_s represents the capacitance of an atomically smooth surface area. The C_{dl} values were determined by the gradient of the graph of capacitive current density against scan rates. The C_s value was adopted as 0.040 mF cm^{-2} in alkaline media and 0.035 mF cm^{-2} in acidic media [26]. Mass activities were calculated using Equation 3.

$$Mass\ activity = j / mass \quad (3)$$

The j denotes the current during the measurements, mass was measured by subtracting from nickel foam after electrochemical deposition to bare nickel foam. The amounts of electrodeposited catalysts were found to be 0.82, 0.81, 0.78, 0.86, and 0.82 mg for MoWNiTe, MoNiTe, WNiTe, NiTe, and Pt/C, respectively.

Turnover frequencies (TOFs) were calculated using Equation 4

$$TOFs = j / 2 \cdot F \cdot n \quad (4)$$

The coefficient 1/2 is originated from the number of electrons required to evolve one H_2 gas, F represents the Faradaic constant (96,485 C mol^{-1}), and n is the number of active sites (mol). The measured loading masses of catalysts were considered active sites and the number of active sites was calculated as follows:

$$MoWNiTe = 0.00082 / (95.95 + 183.84 + 58.69 + 127.60) = 1.76e^{-6} \quad (5)$$

$$MoNiTe = 0.00081 / (95.95 + 58.69 + 127.60) = 2.86e^{-6} \quad (6)$$

$$WNiTe = 0.00078 / (183.84 + 58.69 + 127.60) = 2.10e^{-6} \quad (7)$$

$$NiTe = 0.00086 / (58.69 + 127.60) = 4.61e^{-6} \quad (8)$$

$$Pt/C = 0.00082 / 195.08 = 4.20e^{-6} \quad (9)$$

2.5 Density functional theory calculations

All density functional theory (DFT) calculation here was performed using Quantum Espresso and Perdew-Burke-Ernzerhof (PBE) exchange-correlation functional pseudopotentials were used [27,28]. And meanwhile, Semiempirical Grimme's DFT-D3 dispersion correction was utilized to correct the van der Waals (vdW) interactions [29]. All structures were relaxed with the following sequence: first, vc-relax option was employed to fully relax the whole cell parameters and the positions of atoms. And then, relax option was used to further find the optimized position of each atom with high convergence criteria of force and energy. The cut-off energy here was chosen as 800 Ry which is larger enough to gain the desired result and the Brillouin zone was sampled by a $4 \times 4 \times 1$ Gamma-centered k-paints grid. Another point that should be mentioned was that four layers configuration was modeled and a vacuum layer with a thickness of 15 Å was added along the out-of-plane direction. While the pure NiTe slab model contains four layers, stacking by Ni and Ti elements orderly, the initial cell is expanded into a 2×2 supercell which contains 16 atoms. It is worth mentioning that initial bulk NiTe possesses a hexagonal structure, and its lattice belongs to the space group P63/mmc. Our computed lattice parameter for this structure after optimization was a = 4.042 Å. For the model of MoWNiTe, considering periodicity, centrally located atoms are more likely to be replaced. Therefore, we chose the central position and the position adjacent to it as the substitution sites, doped with Mo and W respectively.

3. Results and discussion

3.1. Material preparation and Characterization

Fig. 1a shows the conceptual schematic of the formation reaction of ternary transition metals-based nickel telluride (MoWNiTe) catalysts as a heterogeneous catalyst system using a simple and facile electrodeposition technique. Generally, as the deposition time increases, the electrodeposition follows the Stranski-Krastanov (SK) growth, leading to a transition from the 2-dimensional (2D) layer growth to the 3D island growth at a critical film thickness [30,31]. This

results in the formation of a 3D island structure, which provides a large surface area useful for electrocatalysis applications. However, as shown in Fig. 1a, the excessive growth of particles can occur through the relatively fast atomic diffusion in the simple component system such as NiTe [32], resulting in an overgrown NiTe with a large particle size. In contrast, in the heterogeneous multi-component system, the atomic diffusion can be more sluggish due to the chemical potential difference between multi-component elements inducing high migration barriers [32-34]. Thus, it is expected that by introducing high valence non-3d metal (single Mo, W, and binary MoW) into the NiTe (as described in the Experimental section), heterogeneous multi-component catalysts, such as MoNiTe or WNiTe and MoWNiTe, can be synthesized and smaller with increasing the number of foreign non-3d metal elements.

As expected, field emission scanning electron microscope (FE-SEM) results showed that the particle size of electrodeposited samples strongly depends on the number of components under the same deposition time (Fig. 1b). It was found that MoWNiTe (~300 nm) has a smaller particle size than MoNiTe (~450 nm), WNiTe (~450 nm), and overgrown NiTe (~5600 nm) (Fig. S1-4). Moreover, Fig. 1c shows X-ray diffraction (XRD) patterns of all the telluride samples prepared by electrodeposition. As shown in Fig. 1c, the broad peak around $2\theta = 31.75°$, which is assigned to the (101) plane of NiTe (ICSD ID 51732), gradually disappeared as more foreign atoms were introduced to the NiTe. This finding suggests that the sluggish atomic diffusion in the multi-component system retards grain growth, leading to a small particle size [32]. Furthermore, aberration-corrected transmission electron microscope (Cs-TEM) examinations were performed to characterize the element composition and microstructure of the electrodeposited samples (Fig. 1d). On the right side of Fig. 1d is the random atomic structure in amorphous MoWNiTe. MoNiTe (Fig. S2) and WNiTe (Fig. S3) show the mixed feature of the ordered and disordered structure, whereas overgrown NiTe (Fig. S4) shows a crystalline feature. These results are well consistent with XRD results showing that heterogeneous catalysts are more amorphized with an increasing number of foreign elements. In addition, it was further confirmed by the energy-dispersive X-ray spectroscopy (EDS) measurements that all the samples show uniform elemental distributions in MoWNiTe (Fig. 1e and Fig. S1), MoNiTe (Fig. S2), WNiTe (Fig. S3), and overgrown NiTe (Fig. S4), respectively. The elemental composition of electrodeposited catalysts determined by inductively coupled plasma atomic emission spectrometer (ICP-AES) is summarized in Table S1.

We investigated the chemical structures and electronic interactions of the electrodeposited

samples using X-ray photoelectron spectroscopy (XPS). Fig. 1f shows high-resolution XPS spectra of Ni 2p, Te 3d, Mo 3d, and W 4f peak regions with the fitted peak components. It can be seen that the ratio of Ni^{2+} and Ni^{3+} states, which are deconvoluted from Ni $2p_{3/2}$ spectra, was found to be 1.21, 1.38, 1.52, and 3.05, for NiTe, MoNiTe, WNiTe, and MoWNiTe, respectively [21-24]. These results indicate that the modification of the electronic structure of MoWNiTe catalysts by the combination of foreign Mo and W metals induces more electron-rich Ni states [35,36], which are more favorable for HER [37,38], compared to MoNiTe or WNiTe modulated by single foreign metal solely and overgrown NiTe catalysts. Furthermore, it was observed that there exist high valence oxidation (Te^{4+} at 575.4 and 585.8 eV and Te^{6+} at 577.3 and 587.3 eV) states, indicating that Te provides a strong oxophilic effect [21-24]. It was also found that in the Mo 3d region, after the incorporation of W into MoNiTe, high valence non-3d transition metal states (Mo^{5+} and Mo^{6+}) increase while Mo^{4+} (229.0 and 232.6 eV) and Mo^{0} states (227.6 and 231 eV) decrease [10,35,39]. W $4f_{7/2}$ (34.9 eV), and W $4f_{5/2}$ (37.0 eV) peaks show a similar trend as the evolution of Mo 3d peaks after the incorporation of Mo into WNiTe [9,35]. These results further confirm that the incorporation of high valence non-3d transition metals play an important role as electron donors in promoting the activation process towards HER by modulating the electronic structure of MoWNiTe [35-38].

3.2. Electrochemical measurements

HER performances were evaluated with three-electrode configurations consisting of the working electrode, Hg/HgO reference electrode, and Pt counter electrode in 1 M KOH. Polarization curves were obtained at a scan rate of 1 mV s^{-1} and calibrated to the reversible hydrogen electrode (RHE) scale (Fig. 2a). As expected, MoWNiTe showed excellent overpotentials of 72 and 125 mV to reach the current density of 10 and 100 mA cm^{-2}, respectively. MoWNiTe exhibits a remarkable HER catalytic activity with an overpotential of 182 mV at a high current density of 1000 mA cm^{-2}, which is much lower than the commercial Pt/C (222 mV). Additionally, the catalytic activity of MoWNiTe is superior to the corresponding MoNiTe, WNiTe, and NiTe, which attained overpotentials of 143, 223, and 247, respectively, to reach the current density of 10 mA cm^{-2}. The HER performance of MoWNiTe catalysts is also estimated using carbon paper and graphite rod as a working electrode and a counter electrode, respectively, and demonstrated excellent activity regardless of electrodes (Fig. S5a).

To investigate HER kinetics and the mechanism of the catalysts, Tafel plots were obtained

from polarization curves around the current density of 100 mA cm^{-2} (Fig. 2b). The Tafel slope of MoWNiTe was determined to be 52 mV dec^{-1}, which is smaller than those of MoNiTe (67 mV dec^{-1}), WNiTe (54 mV dec^{-1}), and NiTe (98 mV dec^{-1}), indicating the transition of the rate-determining kinetics away from the Volmer reaction mechanism. Moreover, MoWNiTe showed negligible difference (Δ 7 mV dec^{-1}) in values of the Tafel slope obtained from around 10 to 100 mA cm^{-2} current density, while the commercial Pt/C had a significant increase in the Tafel slope of 95 mV dec^{-1} (Fig. S5b). It should be noted that the increase in the Tafel slope with overpotential is associated with the sluggish Volmer kinetics in alkaline HER [40]. Thus, we believe that the MoWNiTe follows the Heyrovsky mechanism even at the high current density.

To further evaluate and understand the catalytic activities of the electrodeposited catalysts, electrochemical active surface areas (ECSAs), turnover frequencies (TOFs), and specific activities were calculated. MoWNiTe needs a low overpotential of 170 mV to achieve a TOF value of 0.01 H_2 s^{-1} while MoNiTe, WNiTe, and NiTe require higher overpotentials of 283, 315, and 355 mV, respectively, as shown in Fig. 2c. Fig. 2d shows specific activities of electrocatalysts normalized by ECSAs, which are obtained from double-layer capacitance (C_{dl}) (Fig. S6). To reach the specific current density of 10 mA cm^{-2}, MoWNiTe needs a much lower overpotential of 134 mV compared to MoNiTe (282 mV), WNiTe (322 mV), and NiTe (356 mV). Geometrical current densities, TOFs, and mass activities at - 0.15 V versus RHE are summarized in bar plots, showing that the MoWNiTe has superior extrinsic and intrinsic activities to the other prepared catalysts (Fig. 2e and Fig. S7). Additionally, we compared the performance of MoWNiTe to the recently studied alkaline HER electrocatalysts based on the value of overpotential and Tafel slope at the current density of 10 mA cm^{-2}, as summarized in Table S2, showing comparable or superior performance.

Electrochemical stability tests were carried out with the best-performed MoWNiTe catalyst at the current density of 100 mA cm^{-2} for a long term of 3000 hours in 1 M KOH using chronopotentiometry (CP) (Fig. 2f). MoWNiTe showed no significant change in its performance during the long-term stability test and its polarization curves (inset of Fig. 2f) showed a negligible degradation of Δ 1 mV after stability tests. Moreover, after a long-term HER stability test, it was confirmed from FE-SEM and Cs-TEM measurements that the surface structure and elemental distribution of MoWNiTe were retained, supporting excellent electrochemical stability (Fig. S8). Ex-situ XPS examination results also showed that low valence Te^{2-} and high valence Te^{6+} states, indicating $Te(OH)_6$ species, were simultaneously increased in the Te 3d region (Fig. S9) after a

stability test. Thus, the superior HER catalytic behavior of the optimized MoWNiTe can be explained with the following synergistic benefits: (1) the incorporation of high valence non-3d transition metals (Mo and W), which enhance the surface area with small particle size by sluggish atomic diffusion and the intrinsic catalytic activity by modulating the electronic structure, leading to electron-rich low valence states [37,38]; (2) the oxophilicity of Te as a dominant OH^- adsorption site ($OH^- \leftrightarrow OH_{ad} + e^-$), which leads to accumulation of reactive OH* species on the catalyst surface to promote water dissociation through a bifunctional catalytic mechanism in alkaline media.

In order to further address whether Te with a high oxophilicity can provide bifunctional catalytic sites associated with the in-situ formation of reactive OH* for efficient HER, we evaluated HER activity of MoWNiTe as a function of Te contents (0 – 100 %). As shown in Fig. 3a, HER activity is sensitively dependent on the amount of Te in $MoWNiTe_{1-x}$ (x = 0 ~ 1). HER performance gradually improves as the amount of Te increases from 0 (MoWNi) to 100 % (MoWNiTe). Tafel slopes decrease from 140 to 52 mV dec^{-1} around the current density of 100 mA cm^{-2}, and zeta potential increases from 7.14 to 14.85 mV as the Te content increases from 0 to 100 % (Fig. 3b and Fig. S10). Moreover, from cyclic voltammetry (CV) analysis (Fig. 3c), the Te anodic peak increases as the amount of Te in MoWNiTe increases while the Ni anodic peak decreases, confirming that Te acts as a dominant OH adsorption site ($OH^- \rightarrow OH_{ad} + e^-$) [41]. These findings suggest that introducing the oxophilic Te makes the catalytic surface more positively charged with increasing Te contents. This accelerates the catalytic interaction with OH^-, leading to a transition of the rate-determining step from the Volmer to Heyrovski step (Fig. 3d). Furthermore, density functional theory calculations were conducted to identify the free energy for the water dissociation process in alkaline media as shown in Fig. 3e and Fig. S11. It can be clearly seen that the MoWNiTe exhibits a significantly reduced free energy of 0.536 eV for water dissociation compared with that of the NiTe (0.965 eV). These calculation results suggest that the superior HER performance of MoWNiTe is attributed to synergistic effects associated with the electronic structure modulation through the incorporation of high valence non-3d transition metals and the oxophilicity of Te leading to the accumulation of reactive OH* species on the catalyst surface to accelerate water dissociation through a bifunctional catalytic mechanism.

To demonstrate the high HER catalytic activity of MoWNiTe following the bifunctional mechanism within universal pH conditions, HER measurements of MoWNiTe were further carried out in non-alkaline media. 1 M phosphate-buffered saline (PBS) (pH ~ 7.4) and 0.5 M H_2SO_4 (pH

~ 0.3) electrolytes were used with the same electrochemical setup with Ag/AgCl as the reference electrode. In 1 M PBS, the MoWNiTe exhibited the best HER electrocatalytic performance with a superior overpotential of 45 mV and Tafel slope of 60 mV dec^{-1} at the current densities of 10 mA cm^{-2}, respectively, which are lower than commercial Pt/C and the other electrocatalysts (Fig. 4a,c) as well as previously reported HER electrocatalysts (Table S3). MoWNiTe also showed remarkable overpotentials of 31 and 54 mV and Tafel slope of 34 and 70 mV dec^{-1} at the current densities of 10 and 100 mA cm^{-2}, respectively, (Fig. 4b,d), which are much smaller than those of recently studied non-alkaline HER electrocatalysts and comparable to commercial Pt/C (Table S4). Furthermore, MoWNiTe exhibited the lowest charge transfer resistance among the prepared catalysts in universal pH environments, which is comparable to commercial Pt/C (Fig. S12).

The electrochemical stability of MoWNiTe was also evaluated in both the 1 M PBS and 0.5 M H_2SO_4 electrolytes. CP curves are well retained in both the neutral and acidic media for a long-term of 1000 hours at the current density of 100 mA cm^{-2} (Fig. 4e). Besides, only 4 and 1 mV of overpotential increments were observed at the 100 mA cm^{-2} in 1 M PBS and 0.5 M H_2SO_4, respectively, (Fig. 4f), showing the excellent stability of MoWNiTe. Thus, it is considered that the excellent electrochemical behavior of MoWNiTe within the universal pH range is attributed to synergistic effects of incorporated high valence Mo and W, increasing intrinsic catalytic activity, as well as oxophilic Te, leading to the accumulation of reactive OH* species in high pH environments, which facilitate HER activity through the bifunctional mechanism associated with efficient water dissociation.

4. Conclusion

In this study, we designed and demonstrated a ternary transition metals-based nickel telluride system with high valence non-3d metals (Mo and W) and oxophilic Te as efficient heterogeneous HER electrocatalysts following the bifunctional mechanism. The incorporation of high valence non-3d two hetero-transition metals effectively induced electron-rich low valence states of Ni and Te, leading to the enhanced hydrogen reduction reaction. Furthermore, introducing Te made the catalytic surface more oxophilic, enabling accelerated catalytic interaction with OH-, resulting in a transition of the rate-determining step from the Volmer to the Heyrovski step. As a result, the optimized MoWNiTe showed excellent pH-universal HER performances with overpotentials of 72, 45, and 31 mV at the current density of 10 mA cm^{-2} in alkaline, neutral, and

acid media, respectively, which are much superior or comparable to previously reported electrocatalysts and commercial Pt/C within universal pH environments. In addition, superior long-term catalytic stability of MoWNiTe was also demonstrated without a negligible degradation of overpotential increment up to 3000 hours in alkaline and 1000 hours in non-alkaline media at the current density of 100 mA cm^{-2}. These experimental results are consistent with density functional theory calculations, demonstrating that the enhanced HER performance was due to the reduced free energy for water dissociation. We believe that our findings provide insight into the design of highly efficient and stable HER electrocatalysts in universal pH and new prospects for a bifunctional mechanism.

Declaration of Competing Interest

The authors declare no competing financial interest.

Acknowledgments

This work was supported through the National Research Foundation of Korea (NRF) funded by the Ministry of Science and ICT (2022M3H4A1A04096478). The authors appreciate the support from the Supercomputing Center of Wuhan University.

Appendix A. Supporting Information

FE-SEM and Cs-TEM images, Table for elemental composition of the prepared catalysts, Polarization curves of MoWNiTe with different electrochemical setups, Tafel plots at the current density from 10 to 100 mA cm^{-2}, CV curves in the non-Faradaic region, Table for HER activity in 1 M KOH compared to recently studied electrocatalysts, XPS spectra after long-term stability test, FE-SEM and Cs-TEM images after a long-term stability test, Tafel plots of MoWNiTe with different Te contents, Table for HER activity in 1 M PBS and 0.5 M H_2SO_4 compared to recently studied electrocatalysts, EIS data of the prepared catalysts in universal pH environments.

References

[1] J. Yao, Z. Wu, H. Wang, F. Yang, J. Ren, Z. Zhang, J. Energy Chem. 74 (2022), 218-238

[2] Q. Xu, J. Zhang, H. Zhang, L. Zhang, L. Chen, Y. Hu, H. Jiang, C. Li, Energy Environ. Sci. 14 (2021), 5228-5259

[3] H. J. Kim, H. Y. Kim, J. Joo, S. H. Joo, J. S. Lim, J. Lee, H. Huang, M. Shao, J. Hu, J. Y. Kim, B. J. Min, S. W. Lee, M. Kang, K. Lee, S. Choi, Y. Park, Y. Wang, J. Li, Z. Zhang, J. Ma, S. -I. Choi, J. Mater. Chem. A 10 (2022), 50-88

[4] J. M. -Ibrahim, X. Sun, J. Energy Chem. 34 (2019), 111-160

[5] J. Kim, H. Kim, W. -J. Lee, B. Ruqia, H. Baik, H. -S. Oh, S. -M. Paek, H. -K. Lim, C. H. Choi, S. -I. Choi, J. Am. Chem. Soc. 141 (2019) 45, 18256-18263

[6] W. Li, C. Wang, X. Lu, J. Mater. Chem. A 9 (2021), 3786-3827

[7] L. Su, D. Gong, Y. Jin, D. Wu, W. Luo, J. Energy Chem. 66 (2022), 107-122

[8] J. Kim, H. J. Kim, B. Ruqia, M. J. Kim, Y. J. Jang, T. H. Jo, H. Baik, H. S. Oh, H. S. Chung, K. Baek, S. Noh, M. Jung, K. J. Kim, H. K. Lim, Y. S. Youn, S. I. Choi, Adv. Mater. (2021), 2105248

[9] H. C. Fu, X. H. Fang, X. H. Chen, Q. Zhang, N. B. Li, H. Q. Luo, Appl. Catal. B: Environ. 301 (2021), 120818

[10] Y. Jiang, P. Sun, L. Sharma, B. Mao, R. Kakkar, T. Meng, L. Zheng, M. Cao, Nano Energy 81 (2021), 105645

[11] S. Zhu, X. Qin, F. Xiao, S. Yang, Y. Xu, Z. Tan, J. Li, J. Yan, Q. Chen, M. Chen, M. Shao, Nat. Catal. 4 (2021), 711-718

[12] G. Feng, F. Ning, J. Song, H. Shang, K. Zhang, Z. Ding, P. Gao, W. Chu, D. Xia, J. Am. Chem. Soc. 143 (2021), 41, 17117-17127

[13] S. Ma, J. Deng, Y. Xu, W. Tao, X. Wang, Z. Lin, Q. Zhang, L. Gu, W. Zhong, J. Energy Chem. 66 (2022), 560-565

[14] L. Zhang, Z. Wang, J. Zhang, Z. Lin, Q. Zhang, W. Zhong, G. Wu, Nano Research (2022), https://doi.org/10.1007/s12274-022-5322-2

[15] C. Wang, H. Shang, H. Xu, Y. Du, J. Mater. Chem. A 9 (2021), 857-874

[16] T. Xiong, B. Huang, J. Wei, X. Yao, R. Xiao, Z. Zhu, F. Yang, Y. Huang, H. Yang, M. -S. Balogun, J. Energy Chem. 67 (2022), 805-813

[17] M. Wang, L. Zhang, Y. He, H. Zhu, J. Mater. Chem. A 9 (2021), 5320-5363

[18] Y. Zhao, S. Wei, K. Pan, Z. Dong, B. Zhang, H. H. Wu, Q. Zhang, J. Lin, H. Pang, Chem. Eng. J. 421 (2021), 129645
[19] Z. Y. Yu, Y. Duan, X. Y. Feng, X. Yu, M. R. Gao, S. H. Yu, Adv. Mater. 33 (2021), 2007100
[20] Z. Wang, S. Shen, Z. Lin, W. Tao, Q. Zhang, F. Meng, L. Gu, W. Zhong, Adv. Funct. Mater. 32 (2022), 2112832
[21] M. Yuan, Q. Li, J. Zhang, J. Wu, T. Zhao, Z. Liu, L. Zhou, H. He, B. Li, G. Zhang, Adv. Funct. Mater. 30 (2020), 2004208
[22] L. Hu, X. Zheng, X. Wei, H. Wang, Y. Wu, W. Gu, L. Shi, C. Zhu, Appl. Catal. B: Environ. 273 (2020), 119014
[23] H. Sun, J. M. Yang, J. G. Li, Z. Li, X. Ao, Y. Z. Liu, Y. Zhang, Y. Li, C. Wang, J. Tang, Appl. Catal. B: Environ. 272 (2020), 118988
[24] G. Li, J. Huang, Q. Yang, L. Zhang, Q. Mu, Y. Sun, S. Parkin, K. Chang, C. Felser, J. Energy Chem. 62 (2021), 516-522
[25] S. Jo, K. B. Lee, J. I. Sohn, ACS Sustainable Chem. Eng. 9 (2021), 14911-14917
[26] C. C. L. McCrory, S. Jung, J. C. Peters, T. F. Jaramillo, J. Am. Chem. Soc. 135 (2013), 16977-16987
[27] P. Giannozzi, S. Baroni, N. Bonini, M. Calandra, R. Car, C. Cavazzoni, D. Ceresoli, G. L. Chiarotti, M. Cococcioni, I. Dabo, A. D. Corso, S. Gironcoli, S. Fabris, G. Fratesi, R. Gebauer, U. Gerstmann, C. Gougoussis, A. Kokalj, M. Lazzeri, L. Martin-Samos, N. Marzari, F. Mauri, R. Mazzarello, S. Paolini, A. Pasquarello, L. Paulatto, C. Sbraccia, S. Scandolo, G. Sclauzero, A. P. Seitsonen, A. Smogunov, P. Umari, R. M. Wentzcovitch, J. Phys. Condens. Mat. 21 (2009), 39.
[28] J. P. Perdew, K. Burke, M. Ernzerhof, Phys. Rev. Lett. 77 (1996), 18, 3865-3868.
[29] V. Barone, M. Casarin, D. Forrer, M. Pavone, M. Sambi, A. Vittadini, J. Comput. Chem. 30 (2009), 6, 934-939.
[30] H. Tian, Z. Li, G. Feng, Z. Yang, D. Fox, M. Wang, H. Zhou, L. Zhai, A. Kushima, Y. Du, Z. Feng, X. Shan, Y. Yang, Nat. Commun. 12 (2021), 237
[31] M. Li, M. T. Curnan, M. A. G. -Sill, S. D. House, W. A. Saidi, J. C. Yang, Nat. Commun. 12 (2021), 2781
[32] R. Krishna, Chem. Soc. Rev. 44 (2015), 2812

[33] S. Alvi, D. M. Jarzabek, M. G. Kohan, D. Hedman, P. Jenczyk, M. M. Natile, A. Vomiero, F. Akhtar, ACS Appl. Mater. Interfaces 12 (2020), 18, 21070-21079
[34] D. Luo, Q. Zhou, W. Ye, Y. Ren, C. Greiner, Y. He, H. Wang, ACS Appl. Mater. Interfaces 13 (2021), 46, 55712-55725
[35] Y. Yang, Y. Qian, H. Li, Z. Zhang, Y. Mu, D. Do, B. Zhou, J. Dong, W. Yan, Y. Qin, L. Fang, R. Feng, J. Zhou, P. Zhang, J. Dong, G. Yu, Y. Liu, X. Zhang, X. Fan, Sci. Adv. 6 (2020), eaba6586
[36] B. Zhang, L. Wang, Z. Cao, S. M. Kozlov, F. P. G. Arquer, C. T. Dinh, J. Li, Z. Wang, X. Zheng, L. Zhang, Y. Wen, O. Vonznyy, R. Comin, P. D. Luna, T. Regier, W. Bi, E. E. Alp, C. W. Pao, L. Zheng, Y. Hu, Y. Ji, Y. Li, Y. Zhang, L. Cavallo, H. Peng, E. H. Sargent, Nat. Catal. 3 (2020), 985-992
[37] M. Wang, J. Q. Wang, C. Xi, C. Q. Cheng, C. G. Kuai, X. L. Zheng, R. Zhang, Y. M. Xie, C. K. Dong, Y. J. Chen, X. W. Du, Small 17 (2021), 2100203
[38] H. Ma, Z. Chen, Z. Wang, C. V. Singh, Q. Jiang, Adv. Sci. (2022), 2105313
[39] R. Q. Yao, Y. T. Zhou, H. Shi, W. B. Wan, Q. H. Zhang, L. Gu, Y. F. Zhu, Z. Wen, X. Y. Lang, Q. Jiang, Adv. Funct. Mater. 31 (2021), 2009613
[40] T. Shinagawa, A. T. G. Esparza, K. Takanabe, Sci. Rep. 5 (2015), 13801
[41] W. M. Latimer, Oxidation Potentials. 2nd Ed., Prentice-Hall, New York, 1952

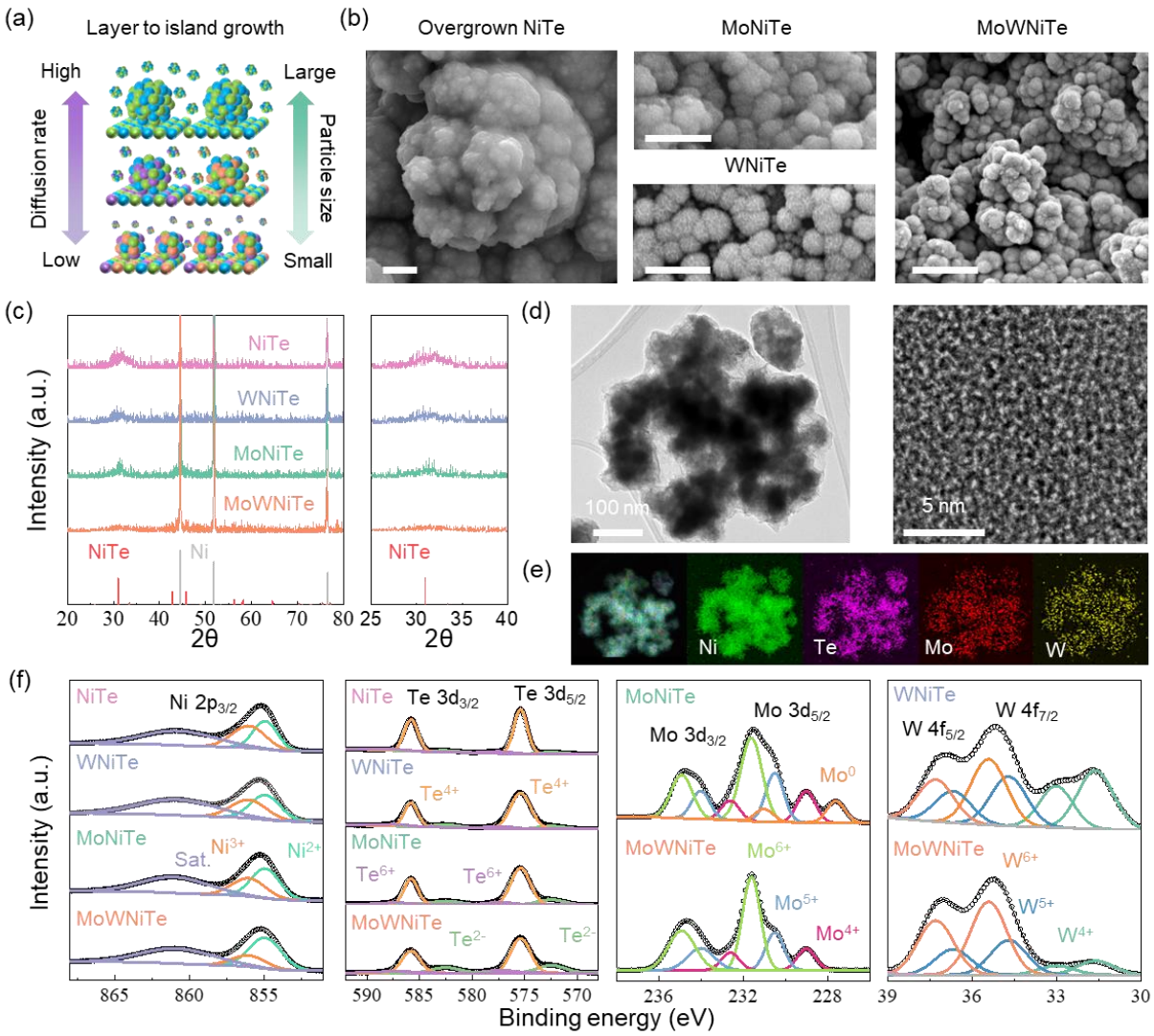

Fig. 1. Characterization of electrodeposited catalysts. (a) Schematic illustration of the formation reaction of the electrocatalyst during electrodeposition. Yellow, blue, purple, and grey particle represent Ni, Te, Mo, and W, respectively. (b) Field emission scanning electron microscope (FE-SEM) images of the electrocatalysts samples (All scale bars, 1 μm). (c) X-ray diffraction (XRD) patterns of the prepared electrocatalysts. (d) Spherical aberration-corrected transmission electron microscope (Cs-TEM), and (e) energy-dispersive X-ray spectroscope (EDS) images of MoWNiTe. (f) X-ray photoelectron spectroscopy (XPS) spectra of the electrocatalysts samples in Ni 2p, Te 3d, Mo 3d, and W 4f peak regions.

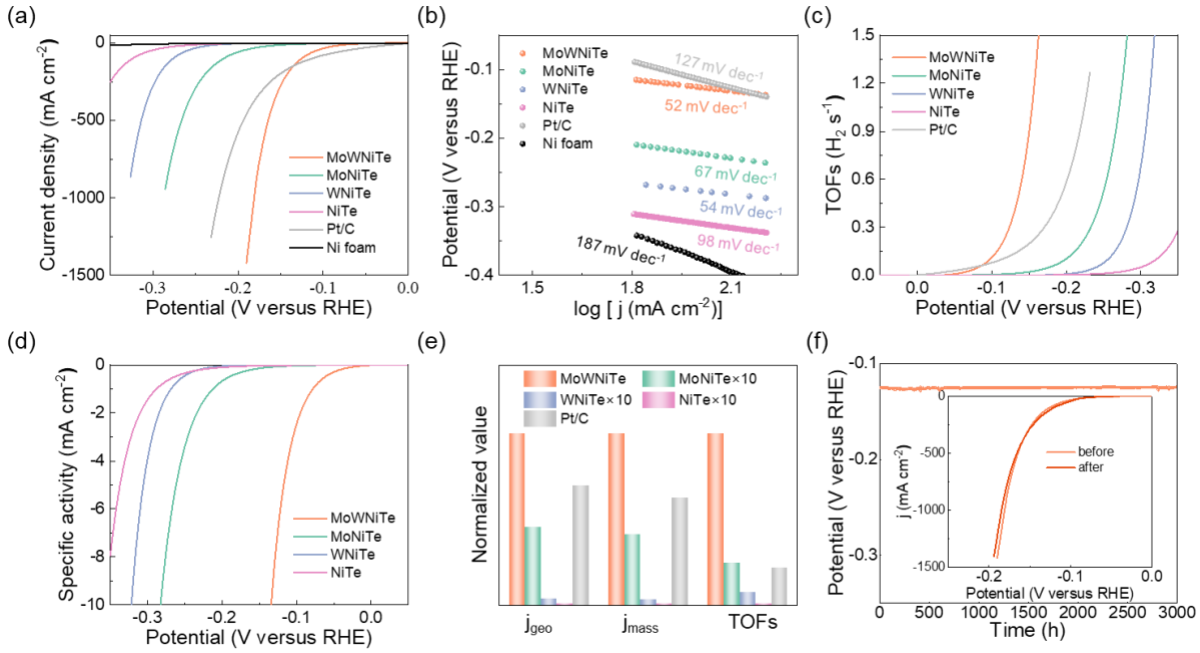

Fig. 2. Electrochemical measurements in 1 M KOH. (a) Polarization curves of the electrodeposited catalysts. (b) Tafel plots of the electrocatalysts around the current density of 100 mA cm^{-2}. (c) Turnover frequencies (TOFs) and (d) specific activity of the prepared electrocatalysts. (e) Bar plots of the electrocatalysts samples summarized with respect to geometrical current densities, mass activities, and TOFs at – 0.15 V versus RHE. The values of MoNiTe, WNiTe, and NiTe were 10 times (denoted as × 10) their original values. (f) Chronopotentiometry (CP) curves of MoWNiTe at the current density of 100 mA cm^{-2}. Inset shows polarization curves of MoWNiTe before and after the stability test.

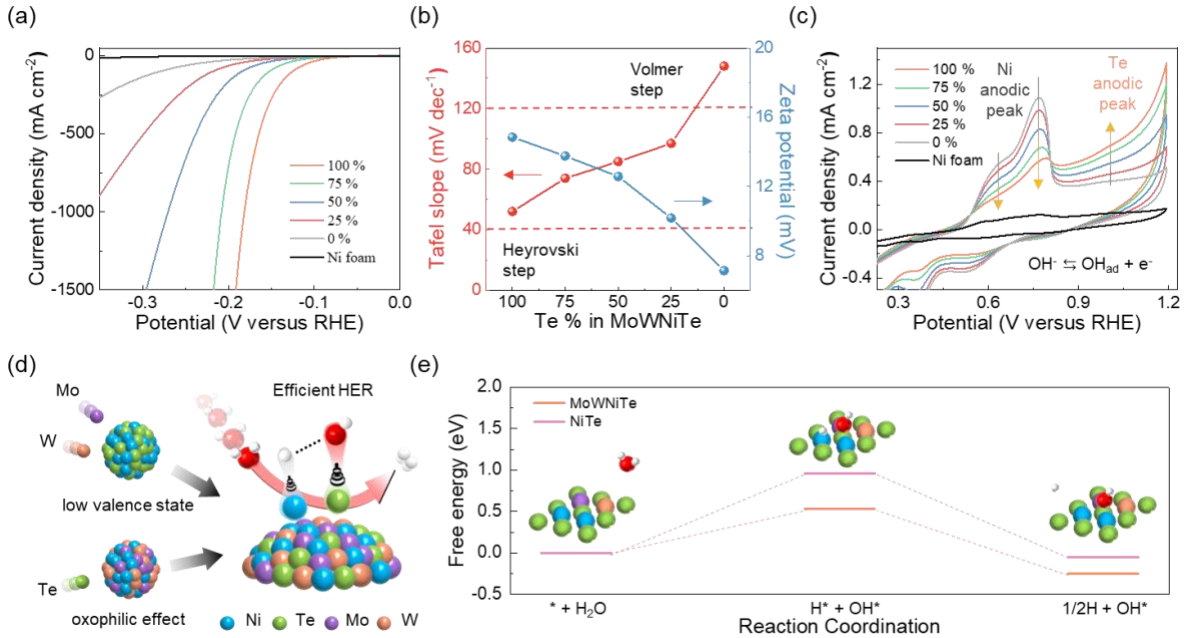

Fig. 3. Catalytic activity of MoWNiTe based on Te contents in 1 M KOH. (a**)** Polarization curves of MoWNiTe with different Te contents. (b) Tafel slope and zeta potential with respect to Te contents in MoWNiTe. (c) Cyclic voltammetry (CV) curves of MoWNiTe with different Te contents with a scan rate of 10 mV s^{-1}. Downward and upward arrows indicate Ni and Te oxidation peaks, respectively. (d) Schematic illustration of water dissociation process on the surface of MoWNiTe in alkaline media. (e) Free energy diagram of HER reactions in alkaline media.

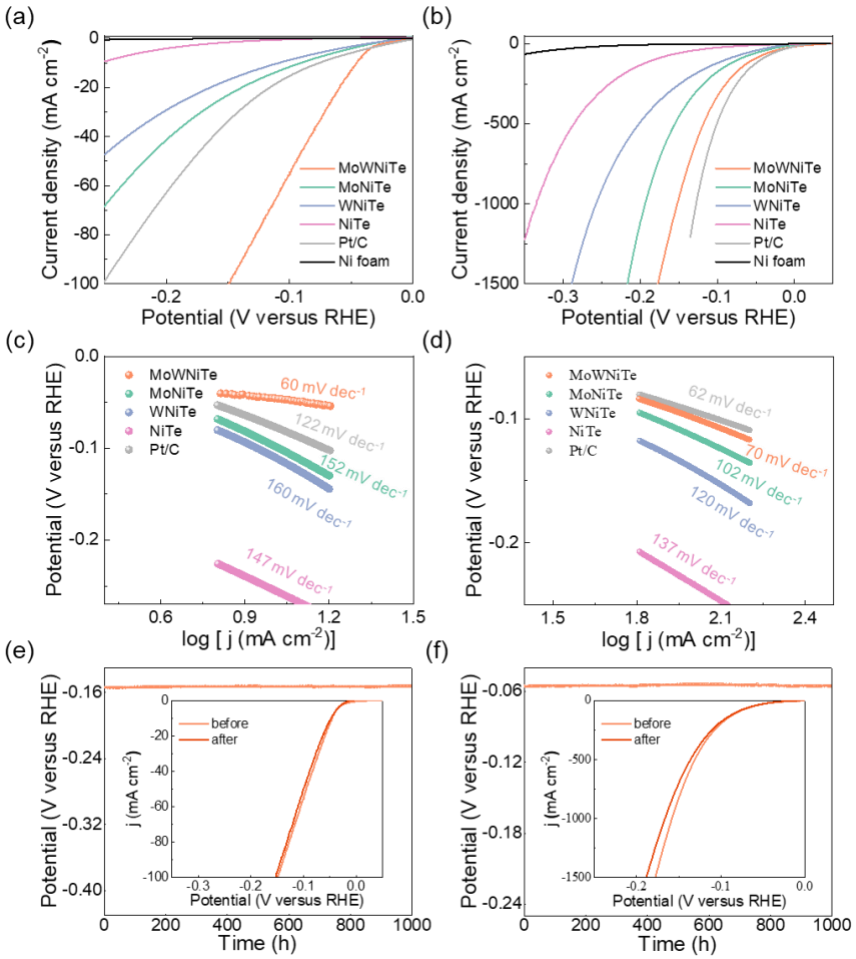

Fig. 4. Electrochemical measurements in 1 M PBS and 0.5 M H_2SO_4. Polarization curves in (a) 1 M PBS, and (b) 0.5 M H_2SO_4. Tafel plots derived from polarization curves in (c) 1 M PBS, and (d) 0.5 M H_2SO_4. Chronopotentiometry curves of MoWNiTe at the current density of 100 mA cm^{-2} in (e) 1 M PBS and (f) 0.5 M H_2SO_4. Insets show polarization curves of MoWNiTe before and after the stability test.

Graphical abstract

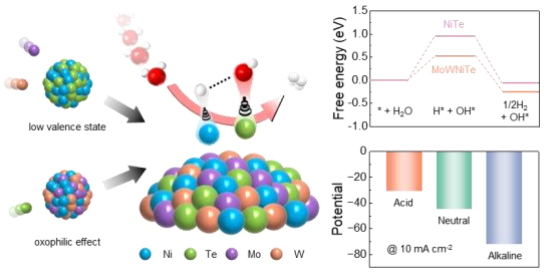

Synergistic effect of high valence Mo and W metals and oxophilic Te in MoWNiTe on accelerating water dissociation for efficient hydrogen evolution reaction in universal pH environments.